Antiferromagnetic superexchange via 3*d* states of titanium in $EuTiO_3$ as seen from hybrid Hartree-Fock density functional calculations

Hirofumi Akamatsu,[1,*] Yu Kumagai,[1] Fumiyasu Oba,[1,†] Koji Fujita,[2] Hideo Murakami,[2] Katsuhisa Tanaka,[2] and Isao Tanaka[1]

[1]*Department of Materials Science and Engineering, Kyoto University, Sakyo, Kyoto 606-8501, Japan*

[2]*Department of Material Chemistry, Kyoto University, Nishikyo, Kyoto 615-8510, Japan*

(Received 10 April 2011; revised manuscript received 15 April 2011; published 15 June 2011)

A superexchange mechanism between Eu^{2+} 4*f* spins via the 3*d* states of nonmagnetic Ti^{4+} ions is proposed through first-principles calculations based on a hybrid Hartree-Fock density functional approach to explain *G*-type antiferromagnetism in $EuTiO_3$. This mechanism is supported by systematic calculations for related Eu^{2+}-based perovskite oxides. In $EuTiO_3$, the competition between the antiferromagnetic superexchange and an indirect ferromagnetic exchange via the Eu 5*d* states leads to a delicate balance between antiferromagnetic and ferromagnetic phases. The superexchange mechanism involving the Ti 3*d* states hints at the microscopic origin of the strong spin-lattice coupling in $EuTiO_3$.

DOI: 10.1103/PhysRevB.83.214421 PACS number(s): 75.30.Et, 71.70.Gm, 75.47.Lx, 75.85.+t

I. INTRODUCTION

The strong cross coupling of multiple degrees of freedom such as spin-lattice coupling is a potential source of robust multiferroicity, which signifies the coexistence of ferromagnetic (FM) and ferroelectric (FE) ordering and the intimate correlation between them. Cubic perovskite $EuTiO_3$ [Fig. 1(a)], which exhibits *G*-type antiferromagnetic (AFM) ordering at 5.3 K[1] and quantum paraelectric (PE) behavior,[2,3] has attracted considerable attention since the discovery of its large magnetoelectric (ME) effect, i.e., a 7% change in the dielectric constant upon the application of a magnetic field of 2 T,[2] implying strong spin-lattice coupling. Previous first-principles studies using the generalized gradient approximation with a $+U$ correction (GGA+U) have predicted that its magnetic ground state is switched from *G*-type AFM to FM with an isotropic increase in the cell volume V[4,5] and that biaxial tensile and compressive strain renders $EuTiO_3$ FM and FE, i.e., multiferroic.[6,7] Experimentally, FM behavior has been reported for an epitaxial $EuTiO_3$ film with a 2%–3% out-of-plane elongation.[8,9] Very recently, an FM and FE phase has been realized in an epitaxial film on a $DyScO_3$ substrate by means of 1.1% biaxial tensile strain.[7] Thus, $EuTiO_3$ is of great interest in that it has a strong spin-lattice coupling and that it is multicritically balanced between the AFM and FM states and between the PE and FE states.

Focusing on its magnetism, the AFM-FM switching in $EuTiO_3$ is viewed as follows: The alignment of two face-centered cubic spin sublattices, in which the Eu^{2+} spins with $S = 7/2$ order ferromagnetically by the next-nearest-neighbor (NNN) interactions, changes from antiparallel (*G*-type AFM) to parallel (FM) depending on the nearest-neighbor (NN) interactions. Therefore, the exchange constant of the NN interactions, J_1, is a key factor in the AFM-FM switching. The mechanism of the sign reversal of J_1, however, remains to be clarified.

In this study, we propose, through hybrid Hartree-Fock density functional calculations, that the 3*d* states of nonmagnetic Ti^{4+} ions introduce a superexchange between the Eu 4*f* spins. This interaction results in an AFM contribution to J_1 and, therefore, plays a critical role in the AFM-FM switching. The superexchange mechanism is corroborated by systematic calculations for a series of Eu^{2+}-based perovskite oxides, i.e., $EuMO_3$ (M = Ti, Zr, Hf, Si, and Ge)[10] and Eu_2TiO_4. It also provides an insight into the microscopic origin of the large ME effect associated with the strong spin-lattice coupling in $EuTiO_3$.[2]

II. COMPUTATIONAL METHODS

The calculations were performed using the HSE06 hybrid functional[12–14] and the projector augmented wave (PAW) method[15] as implemented in the VASP code.[16–20] In the HSE06 hybrid functional, one-quarter of the exchange energy in the Perdew-Burke-Ernzerhof generalized gradient approximation (PBE-GGA)[21] is replaced with the nonlocal Fock exchange, and a screening parameter of 0.208 $Å^{-1}$ is taken. The hybrid Hartree-Fock density functional approach has been shown to lead to a more precise description of the electronic structure for a variety of molecules and solids than that obtained from the local and semilocal functionals,[12–14,19,20,22–27] and this also holds for $EuTiO_3$, as shown later. The PAW data sets with radial cutoffs of 1.5, 1.2, 0.8, 1.3, 1.0, 1.4, and 0.8 Å for Eu, Ti, Si, Zr, Ge, Hf, and O, respectively, were used with a plane-wave cutoff energy of 550 eV. Eu 4*f*, 5*s*, 5*p*, 6*s*; Ti 3*s*, 3*p*, 3*d*, 4*s*; Si 3*s*, 3*p*; Ge 3*d*, 4*s*, 4*p*; Zr 4*s*, 4*p*, 4*d*, 5*s*; Hf 5*p*, 5*d*, 6*s*; and O 2*s*, 2*p* states were described as valence electrons.

The supercell was chosen to be sufficiently large to extract the effective exchange constants for the NN and NNN exchange paths. A $\sqrt{2} \times \sqrt{2} \times 2$ tetragonal supercell containing 20 atoms, illustrated in Fig. 1(a), was adopted for $EuMO_3$ (M = Ti, Si, and Ge) to model three magnetic configurations, i.e., *A*, *F*, and *G* type [Fig. 1(c)]. An orthorhombic unit cell possessing 20 atoms with a space group of *Pbnm*, shown in Fig. 1(b), was used for $EuMO_3$ (M = Zr and Hf) since $EuZrO_3$ has this structure[28] and the same structure has been reported for $SrHfO_3$,[29] which contains Sr^{2+} ions with an ionic radius similar to that of Eu^{2+} ions. A $3 \times 3 \times 2$ *k*-point mesh was used for $EuMO_3$ (M = Ti, Zr, Hf, Si, and Ge) in accordance with the Monkhorst-Pack scheme.[30] A $2 \times 2 \times 1$ supercell consisting of 56 atoms and a $2 \times 2 \times 1$ *k*-point mesh were used for Eu_2TiO_4 with seven magnetic configurations as shown in Fig. 2. The lattice constants and internal coordinates were

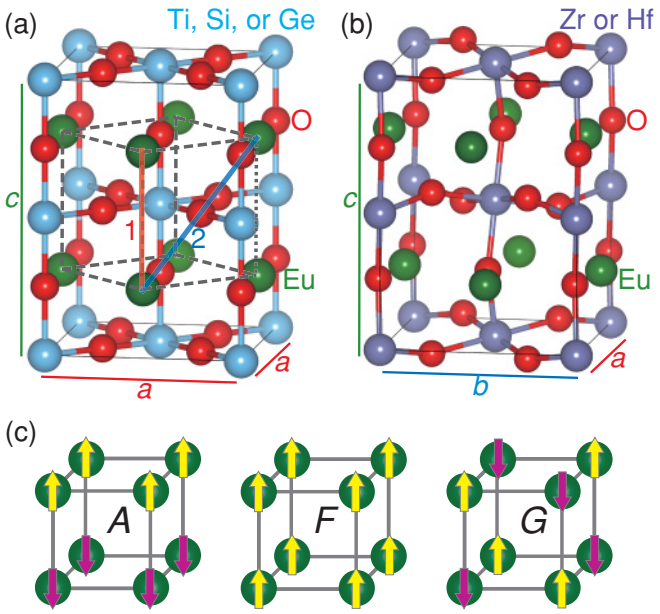

FIG. 1. (Color online) Representations of (a) $\sqrt{2} \times \sqrt{2} \times 2$ tetragonal supercell adopted for EuMO_3 (M = Ti, Si, and Ge) and (b) orthorhombic unit cell adopted for EuMO_3 (M = Zr and Hf) (Ref. 11). The broken lines in (a) represent a cubic unit cell. The numbers 1 and 2 refer to the NN and NNN exchange paths, respectively. (c) Schematics of A-, F-, and G-type magnetic configurations.

optimized until the residual stress and force converged to less than 0.3 GPa and 0.05 eV/Å, respectively.

The NN and NNN exchange constants were calculated by mapping the total energy difference between different magnetic configurations onto the Heisenberg Hamiltonian $H = -2\sum_{i>j} J_{ij}\mathbf{S}_i \cdot \mathbf{S}_j$, where J_{ij} is the exchange constant of magnetic interactions between the Eu 4f spins at the i and j sites and $\mathbf{S}_i$ is the spin vector at the i site.

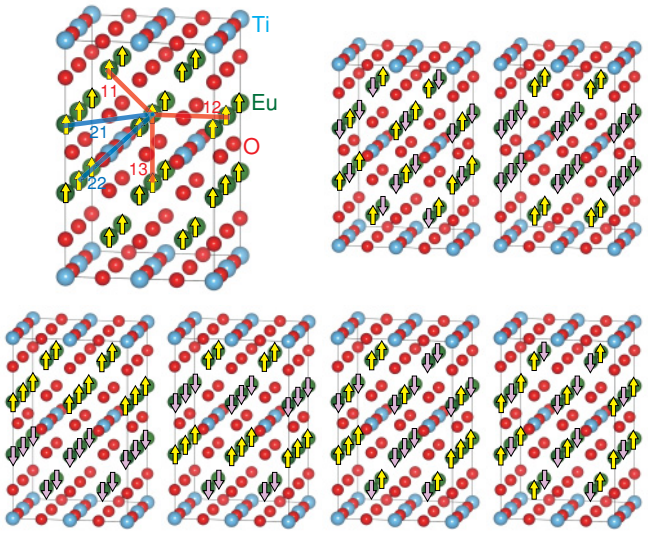

FIG. 2. (Color online) Schematics of $2 \times 2 \times 1$ supercells with seven magnetic configurations adopted for Eu_2TiO_4 (Ref. 11). The numbers $1m$ ($m = 1, 2, 3$) and $2n$ ($n = 1, 2$) refer to the three and two types of NN and NNN exchange paths, respectively.

Here, it should be noted that in the case of EuMO_3 (M = Ti, Si, and Ge), not all the NN and NNN Eu pairs are equivalent in terms of the tetragonal symmetry of the unit cell, respectively. After the structural optimization for the unit cell, however, the ratio of the long to short lattice constants was kept to be almost $\sqrt{2}$ and, thereby, all the distances between the NN Eu ions and between the NNN Eu ions were almost the same, respectively. Therefore, all the NN and NNN exchange constants can be regarded as J_1 and J_2, respectively. On the other hand, since $EuZrO_3$ and $EuHfO_3$ have pseudocubic perovskite structures, they have three and four types of NN and NNN exchange paths, respectively. For these compounds, J_1 and J_2 denote the mean values of the exchange constants for the NN and NNN paths, respectively.

III. RESULTS AND DISCUSSION

Figure 3(a) shows the V dependence of the total energies for $EuTiO_3$ with the A- and F-type magnetic configurations relative to that with the G type. The magnetic ground state is G-type AFM, which is consistent with the experimental observation for bulk $EuTiO_3$. The equilibrium volume of $V = 237.8$ Å^3 at $\Delta V = 0\%$ is in excellent agreement with the experimental volume of 238 Å^3.[2] As V is increased, the magnetic ground state is switched from the G type to the F type, similarly to in previous reports based on the GGA+U approach.[5] Figure 3(b) illustrates the NN and NNN exchange constants, J_1 and J_2, respectively, as a function of V. At $\Delta V = 0\%$, the calculated exchange constants of $J_1 = -0.023$ K and $J_2 = +0.092$ K closely reproduce the experimental values of $J_1 = -0.014$ K and $J_2 = +0.037$ K.[31] A tendency to overestimate exchange constants has also been found in previous hybrid Hartree-Fock density functional studies for other systems.[27] The value of J_1 increases from negative to positive with increasing V, while J_2 is positive over the whole volume range. The reversal of the sign of J_1 is accompanied by the switching of the magnetic ground state from G-type AFM to F-type FM since the total energy difference between the F- and G-type magnetic configurations, $E_F - E_G$, is represented as $-48J_1S(S+1)$. The sign reversal of J_1 implies that some multiple exchange mechanisms are competing for the NN exchange path.

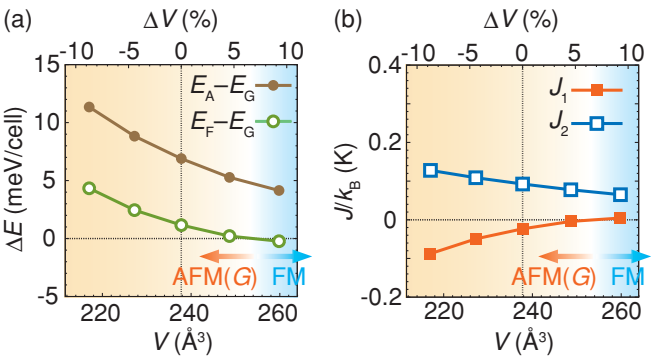

FIG. 3. (Color online) (a) Total energies for the A- and F-type magnetic configurations relative to that for the G type as a function of V for $EuTiO_3$. (b) Variation of J_1 and J_2 with V.

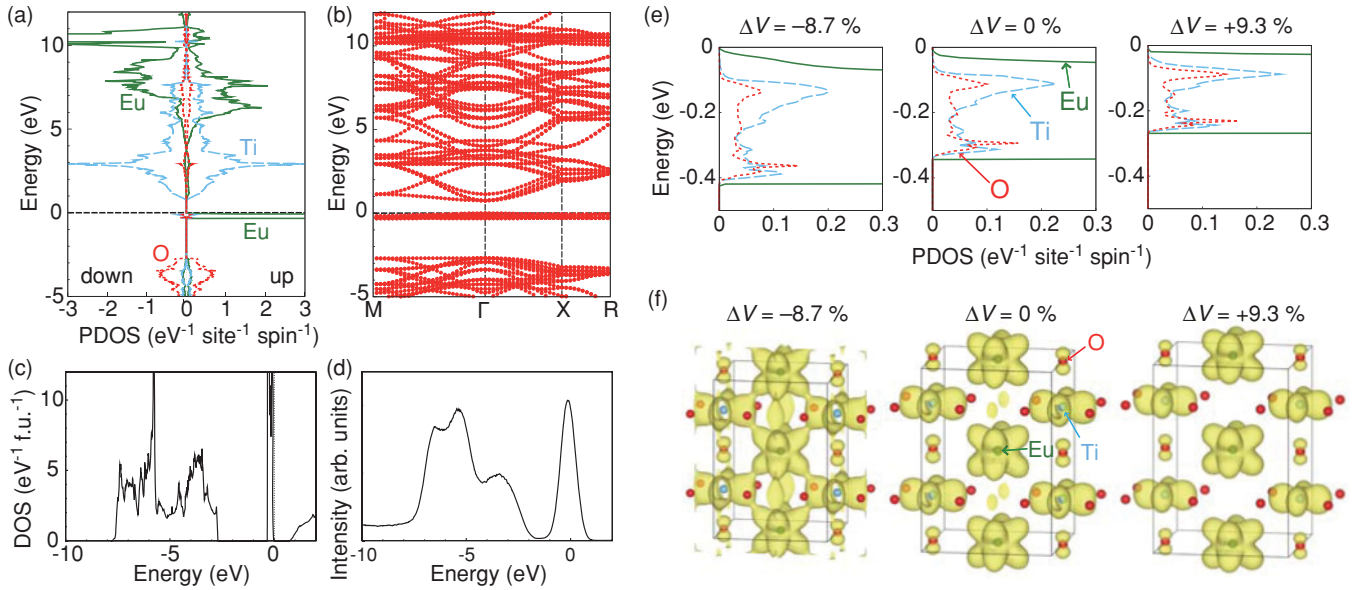

FIG. 4. (Color online) (a) Site-projected PDOS and (b) band structure for $EuTiO_3$ with the *G*-type magnetic configuration at $\Delta V = 0\%$. The PDOS of Eu is for an Eu site with up 4*f* spins. The zero of energy is placed at the highest occupied state. The symmetry points are based on the $\sqrt{2} \times \sqrt{2} \times 2$ supercell. (c) Total DOS for $EuTiO_3$ with the *G*-type magnetic configuration in the energy region near the valence band. (d) HX-PES spectrum for an $EuTiO_3$ thin film. The energy in the HX-PES spectrum is shifted so as to match the peak of the Eu 4*f* states with that in the DOS. (e) Magnified view of the up-spin component of the PDOS in the energy region near the Eu 4*f* band for the *G* type at $\Delta V = -8.7\%$, 0%, and +9.3%. (f) Charge-density isosurfaces for an Eu 4*f* state at the Γ point at 0.003 Å^{-3} for the *G* type (Ref. 11).

An analysis of the electronic structure of $EuTiO_3$ reveals the origin of the exchange interaction. Figure 4(a) illustrates the site-projected partial density of states (PDOS) of $EuTiO_3$ with the *G*-type magnetic configuration at $\Delta V = 0\%$. The valence band mainly consists of O 2*p* states, while the conduction band chiefly has Ti 3*d* and Eu 5*d* characters. Occupied Eu 4*f* bands lying between these bands are narrow, indicating their localized nature. From the band structure shown in Fig. 4(b), the band gap is determined to be 0.85 eV, which is in good agreement with that estimated from an optical absorption spectrum, i.e., 0.93 ± 0.07 eV.[32]

To further verify the calculated electronic structure, the total DOS is compared with the hard x-ray photoelectron spectroscopy (HX-PES) spectrum of $EuTiO_3$ thin films.[33] Figures 4(c) and 4(d) show the total DOS for the *G*-type magnetic configuration and the HX-PES spectrum, respectively. The energy in the HX-PES spectrum is shifted so that the peak of the Eu 4*f* states in the HX-PES spectrum coincides with that in the DOS. The peak positions can be compared between the calculated DOS and the experimental HX-PES spectrum, although the photoionizaton cross sections, which affect peak intensity, are not taken into account. The main component of the DOS in the energy region from −8 to −3 eV is the O 2*p* states and that from −0.5 to 0 eV is the Eu 4*f* states, as seen in Fig. 4. The calculated DOS closely reproduces the positions of the three major peaks in the O 2*p* band and the positional relationship between the O 2*p* and Eu 4*f* states. On the other hand, GGA+*U* with $U_{\text{eff}} = 6.0$ eV underestimates the energy difference between the Eu 4*f* peak and the three major peaks of the O 2*p* states by about 1 eV.[4] Thus, the HSE06 hybrid functional provides a better description of the electronic structure of $EuTiO_3$.

The enlarged view of the PDOS in the energy region near the Eu 4*f* band is depicted for $\Delta V = -8.7\%$, 0%, and +9.3% in Fig. 4(e). The Eu 4*f* states possessing localized spins are hybridized with the Eu 5*d*, Ti 3*d*, and O 2*p* states, and the hybridization among these states becomes stronger as *V* is decreased.

Now let us consider the mechanisms involved in the NN exchange interaction on the basis of the hybridization at the Eu 4*f* band as well as the local ion configuration around the NN Eu^{2+} pairs. As illustrated in Fig. 1(a), there are no intervening ions on the line connecting the NN Eu ions (path 1), while four Ti ions and four O ions lie on the vertical plane between the NN Eu ions. Therefore, possible exchange mechanisms for J_1 are as follows:

(i) *A direct exchange between Eu 4f states.* This interaction is considered to be very weak because there is little direct overlap between Eu 4*f* states, as implied by the narrow width of the Eu 4*f* band.[34,35]

(ii) *An indirect exchange via Eu 5d states.* As discussed in many papers, this indirect exchange is FM and important in Eu^{2+}-based compounds.[31,36] It has been demonstrated experimentally and theoretically that this interaction has the largest contribution to J_1 in Eu chalcogenides; the value of J_1 increases with decreasing *V* due to the predominance of this mechanism.[34,37] The indirect FM exchange should also occur in $EuTiO_3$.[31] However, the value of J_1 is negative at $\Delta V = 0\%$ and decreases with decreasing *V*, in sharp contrast to the case of Eu chalcogenides. It has been suggested that the Ti 3*d* states hybridize with the Eu 5*d* states so as to raise the Eu 5*d* band in $EuTiO_3$, diminishing this interaction.[5] The negative value of J_1 is nonetheless unexplainable. The indirect FM exchange via Eu 5*d* states must compete with some AFM exchange mechanism, leading to the sign reversal of J_1.

(iii) *A superexchange via O 2p states.* It has been claimed that the superexchange for the 90° Eu-O-Eu configuration is AFM and that this AFM superexchange prevails against the indirect FM exchange mentioned above.[1] However, this has been conjectured without theoretical verification; both its sign and magnitude have not been evaluated. As revealed later, the superexchange via O ions is of little significance for the antiferromagnetism of $EuTiO_3$.

(iv) *A superexchange via Ti 3d states.* Here, we propose that an AFM superexchange via Ti 3*d* states is a plausible candidate for an AFM exchange mechanism competing with the indirect FM exchange. Figure 4(f) shows the charge density of the Eu 4*f* state having the strongest mixing with Ti 3*d* states. The Eu 4*f* state is nonorthogonal to the Ti 3*d* states. In the framework of Anderson's superexchange theory,[38] AFM coupling is stabilized by the nonorthogonal overlap between magnetic orbitals mediated by intervening orbitals such as anion *p* states. Therefore, the superexchange via the Ti 3*d* states is expected to be AFM. In Fig. 4(f), the charge density in the area between the Eu and Ti sites increases with a decrease in *V*, which enhances the AFM superexchange. The sign reversal of J_1, as can be seen in Fig. 3(b), is due to the competition between the indirect FM exchange via the Eu 5*d* states and the AFM superexchange via the Ti 3*d* states.

One may also think of a super-superexchange mechanism involving Eu-O-Ti-O-Eu paths. However, almost all the Ti 3*d* states hybridizing with Eu 4*f* states have the t_{2g} symmetry and form π-bonding or nonbonding states with O 2*p* states, resulting in a small value of the transfer integral. In addition, shown in Fig. 4(a), the energy difference between the Eu 4*f* and O 2*p* states and that between the Ti 3*d* and O 2*p* states are much larger than that between the Eu 4*f* and Ti 3*d* states, resulting in a smaller perturbation energy for this super-superexchange. Therefore, the Eu-O-Ti-O-Eu super-superexchange is considered to be weak compared to the Eu-Ti-Eu superexchange although it cannot be completely ruled out.

To determine the scenario of the AFM superexchange via the Ti 3*d* states, we have performed systematic calculations of the exchange interaction for EuMO_3 (M = Zr, Hf, Si, and Ge). The resultant J_1 and J_2 values are shown as a function of *V* in Fig. 5. The *V* dependence of J_1 exhibits different behavior depending on whether the B-site cation belongs to group 4 (M = Zr and Hf) or 14 (M = Si and Ge). For M = Zr and Hf, J_1 is negative and the magnetic ground state is *G*-type AFM at $\Delta V = 0\%$, similarly to $EuTiO_3$. Indeed, a recent experimental study has revealed that $EuZrO_3$ exhibits *G*-type AFM ordering at 4.1 K.[28] The value of J_1 is increased with an increase in *V* as in the case of $EuTiO_3$. On the other hand, for M = Si and Ge, J_1 is positive and the magnetic ground state is FM at $\Delta V = 0\%$. The value of J_1 is decreased with an increase in *V*, contrary to the behavior for M = Ti, Zr, and Hf. A striking difference in the electronic structure of EuMO_3 is the characters of their conduction bands. In the case of M = Ti, Zr, and Hf, the conduction band has the *d* character of the B-site cation, i.e., Ti 3*d*, Zr 4*d*, and Hf 5*d* characters, respectively, while for M = Si and Ge, the conduction band is composed of the *s* state of the B-site cation, i.e., Si 3*s* and Ge 4*s* states, respectively. In $EuZrO_3$ and $EuHfO_3$, the Zr 4*d* and Hf 5*d* states hybridize with the Eu 4*f* states similarly to the Ti 3*d* states in $EuTiO_3$, leading

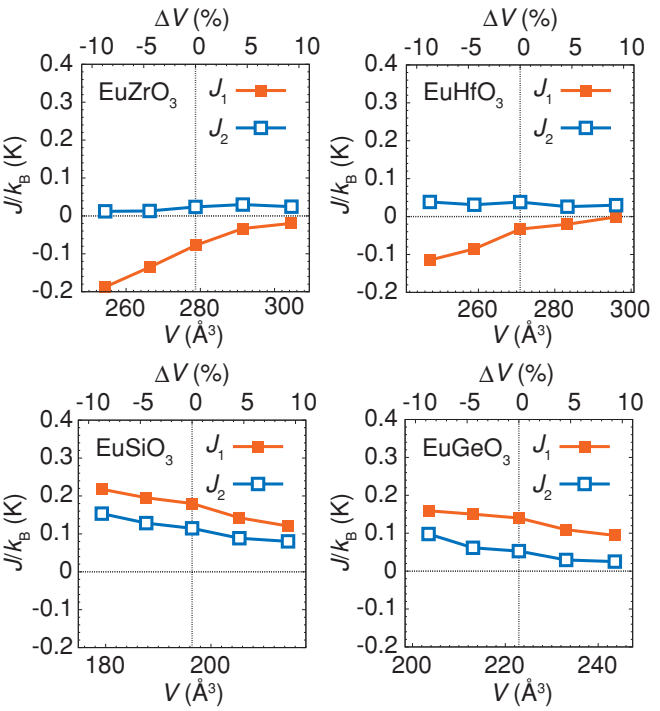

FIG. 5. (Color online) Dependence of J_1 and J_2 on *V* for EuMO_3 (M = Zr, Hf, Si, and Ge). In the case of $EuZrO_3$ and $EuHfO_3$ with pseudocubic structures, J_1 and J_2 indicate the mean values of the NN and NNN exchange constants, respectively.

to the NN AFM superexchange competing with the indirect FM exchange via the Eu 5*d* states. Meanwhile, the indirect FM exchange is predominant in $EuSiO_3$ and $EuGeO_3$, as in the case of Eu chalcogenides, resulting in the FM ground state. Thus, the systematic calculations for EuMO_3 support the AFM superexchange mechanism via the *d* states of the B-site cation in Eu^{2+} perovskite oxides. Moreover, these results exclude the possibility that the main AFM contribution to J_1 is the 90° Eu-O-Eu superexchange, since this interaction exists in EuMO_3 for all M.

The AFM superexchange mechanism is also supported by a calculation for Ruddlesden-Popper phase Eu_2TiO_4, in which EuO and $EuTiO_3$ layers are stacked alternatively. Figure 2 shows the three and two types of NN and NNN exchange paths, referred to as $1m$ (m = 1, 2, 3) and $2n$ (n = 1, 2), respectively.[31] Focusing on the NN exchange paths, paths 11 and 13 are located within the EuO and $EuTiO_3$ layers, respectively, and path 12 is present at the interface between the two layers. The number of Eu-Ti-Eu bridges, which equals the number of Ti ions lying on the vertical plane between the NN Eu ions, is increased from 0 to 2 to 4 moving from path 11 to 12 to 13. Figure 6 illustrates the *V* dependence of the effective exchange constants for the NN and NNN paths, J_{1m} (m = 1, 2, 3) and J_{2n} (n = 1, 2), respectively. The value of J_{11} is decreased with an increase in *V*, similarly to the behavior of J_1 for EuMO_3 with M = Si and Ge. Meanwhile, J_{13} is increased when *V* is increased as in the case of J_1 for EuMO_3 with M = Ti, Zr, and Hf. The value of J_{12} exhibits intermediate behavior between those of J_{11} and J_{13}; J_{12} remains almost constant. Thus, the *V* dependence of the NN interactions is closely related to the local ion configuration. This trend can be interpreted as follows:

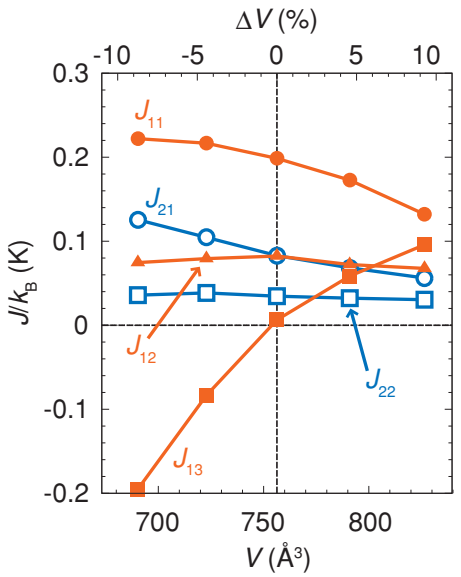

FIG. 6. (Color online) Variation of the exchange constants for the NN interactions, J_{1m} ($m = 1, 2, 3$), and the NNN interactions, J_{2n} ($n = 1, 2$), with V, denoted in Fig. 2.

As the number of Eu-Ti-Eu bridges is increased (moving from J_{11} to J_{12} to J_{13}), the contribution of the Eu-Ti-Eu AFM superexchange is enhanced. Therefore, these results also reinforce the AFM superexchange mechanism via the Ti 3*d* states.

In addition to the context of the isotropic increase in V discussed above, we found that the magnetic ground state is switched from AFM to FM for $EuTiO_3$ both when the lattice constant a is increased with the lattice constant c relaxed and when c is increased with a fixed, which agrees well with the experimental observation of the FM behavior in epitaxial $EuTiO_3$ thin films with biaxial tensile strain[7] and out-of-plane lattice elongation.[8,9] These results can also be understood in terms of the change of the hybridization between the Eu 4*f* and Ti 3*d* states due to the lattice deformation.

Finally, the relationship between the large ME effect of $EuTiO_3$[2] and the superexchange proposed here is briefly mentioned. In $EuTiO_3$, the soft phonon mode that contributes to the largest dielectric weight to the phonon spectrum and hence dominates the ME effect is the Slater mode,[6,7,39] which involves the vibration of Ti^{4+} ions against the O^{2-} octahedra. The spin alignments of Eu^{2+} ions can have a significant impact on the dielectric constant through the Eu-Ti-Eu AFM superexchange, while the impact of the Eu-O-Eu superexchange is considered to be small because of its small contribution to the AFM-FM switching behavior. Thus, the AFM superexchange via the Ti 3*d* states is likely to be one of the microscopic origins of the large ME effect in $EuTiO_3$ as well as the Dzyaloshinskii-Moriya interactions as discussed in Ref. 40.

IV. SUMMARY

We propose a scenario of the AFM superexchange mediated by the Ti 3*d* states between the Eu^{2+} ions in $EuTiO_3$ based on hybrid Hartree-Fock density functional calculations. The AFM superexchange competes with the indirect FM exchange via the Eu 5*d* states, which is responsible for the AFM-FM switching due to the change in V. The NN exchange constants depend on the number of Eu-Ti-Eu bridges in Eu_2TiO_4. The Zr 4*d* and Hf 5*d* states also mediate the AFM superexchanges in $EuZrO_3$ and $EuHfO_3$, respectively, and thereby the superexchange mechanism is generalized to the AFM superexchange via the *d* states of the B-site cation. The AFM superexchange involving the Ti 3*d* states provides an insight into the microscopic origin of the large ME effect observed in $EuTiO_3$.

ACKNOWLEDGMENTS

The authors would like to thank E. Ikenaga and K. Uesugi at the BL47XU beamline of Spring-8 for their technical support (Proposal No. 2010A1652). This research was supported by Grants-in-Aid for Scientific Research on Priority Areas (No. 474) and Scientific Research (A) from MEXT and for JSPS Fellows (No. 22-1280) from JSPS.

*hirofumi.akamatsu@kt4.ecs.kyoto-u.ac.jp
†oba@cms.mtl.kyoto-u.ac.jp

[1] T. R. McGuire, M. W. Shafer, R. J. Joenk, H. A. Alperin, and S. J. Pickart, J. Appl. Phys. **37**, 981 (1966).
[2] T. Katsufuji and H. Takagi, Phys. Rev. B **64**, 054415 (2001).
[3] K. Z. Rushchanskii, S. Kamba, V. Goian, P. Vanek, M. Savinov, J. Prokleska, D. Nuzhnyy, K. Knizek, F. Laufek, S. Eckel *et al.*, Nature Mater. **9**, 649 (2010).
[4] R. Ranjan, H. S. Nabi, and R. Pentcheva, J. Phys. Condens. Matter **19**, 406217 (2007).
[5] R. Ranjan, H. S. Nabi, and R. Pentcheva, J. Appl. Phys. **105**, 053905 (2009).
[6] C. J. Fennie and K. M. Rabe, Phys. Rev. Lett. **97**, 267602 (2006).
[7] J. H. Lee, L. Fang, E. Vlahos, X. Ke, Y. W. Jung, L. F. Kourkoutis, J.-W. Kim, P. J. Ryan, T. Heeg, M. Roeckerath *et al.*, Nature (London) **466**, 954 (2010).
[8] K. Kugimiya, K. Fujita, K. Tanaka, and K. Hirao, J. Magn. Magn. Mater. **310**, 2268 (2007).
[9] K. Fujita, N. Wakasugi, S. Murai, Y. Zong, and K. Tanaka, Appl. Phys. Lett. **94**, 062512 (2009).
[10] The synthesis of EuMO_3 for M = Hf, Si, and Ge has not been reported.
[11] Visualized using the VESTA code (Ref. 41).
[12] J. Heyd, G. E. Scuseria, and M. Ernzerhof, J. Chem. Phys. **118**, 8207 (2003).
[13] J. Heyd, G. E. Scuseria, and M. Ernzerhof, J. Chem. Phys. **124**, 219906 (2006).
[14] A. V. Krukau, O. A. Vydrov, A. F. Izmaylov, and G. E. Scuseria, J. Chem. Phys. **125**, 224106 (2006).
[15] P. E. Blöchl, Phys. Rev. B **50**, 17953 (1994).
[16] G. Kresse and J. Hafner, Phys. Rev. B **48**, 13115 (1993).
[17] G. Kresse and J. Furthmüller, Phys. Rev. B **54**, 11169 (1996).
[18] G. Kresse and D. Joubert, Phys. Rev. B **59**, 1758 (1999).

[19]J. Paier, M. Marsman, K. Hummer, G. Kresse, I. C. Gerber, and J. G. Angyan, J. Chem. Phys. **124**, 154709 (2006).
[20]J. Paier, M. Marsman, K. Hummer, G. Kresse, I. C. Gerber, and J. G. Angyan, J. Chem. Phys. **125**, 249901 (2006).
[21]J. P. Perdew, K. Burke, and M. Ernzerhof, Phys. Rev. Lett. **77**, 3865 (1996).
[22]K. N. Kudin, G. E. Scuseria, and R. L. Martin, Phys. Rev. Lett. **89**, 266402 (2002).
[23]C. Franchini, V. Bayer, R. Podloucky, J. Paier, and G. Kresse, Phys. Rev. B **72**, 045132 (2005).
[24]F. Oba, A. Togo, I. Tanaka, J. Paier, and G. Kresse, Phys. Rev. B **77**, 245202 (2008).
[25]F. Oba, A. Togo, I. Tanaka, K. Watanabe, and T. Taniguchi, Phys. Rev. B **81**, 075125 (2010).
[26]F. Oba, M. Choi, A. Togo, A. Seko, and I. Tanaka, J. Phys. Condens. Matter **22**, 384211 (2010).
[27]A. Meyer, W. F. Perger, R. Demichelis, B. Civalleri, and R. Dovesi, Int. J. Quantum Chem. **110**, 2192 (2010).
[28]Y. Zong, K. Fujita, H. Akamatsu, S. Murai, and K. Tanaka, J. Solid State Chem. **183**, 168 (2010).
[29]B. J. Kennedy, C. J. Howard, and B. C. Chakoumakos, Phys. Rev. B **60**, 2972 (1999).
[30]H. J. Monkhorst and J. D. Pack, Phys. Rev. B **13**, 5188 (1976).
[31]C.-L. Chien, S. DeBenedetti, and F. D. S. Barros, Phys. Rev. B **10**, 3913 (1974).
[32]J. H. Lee, X. Ke, N. J. Podraza, L. F. Kourkoutis, T. Heeg, M. Roeckerath, J. W. Freeland, C. J. Fennie, J. Schubert, D. A. Muller *et al.*, Appl. Phys. Lett. **94**, 212509 (2009).
[33]$EuTiO_3$ thin films were grown on $SrTiO_3$ (001) substrates by pulsed laser deposition (PLD). Details of the growth conditions have been reported in Ref. 9. HX-PES measurement was performed at the BL47XU beamline of SPring-8. The HX-PES spectrum was taken at room temperature with an excitation energy of 7.94 keV. The total energy resolution was set to 250.06 meV. The take-off angle of photoelectrons was set at 88° to reduce the effect of surface contamination on the HX-PES spectrum.
[34]J. Kunes, W. Ku, and W. E. Pickett, J. Phys. Soc. Jpn. **74**, 1408 (2005).
[35]T. Kasuya, IBM J. Res. Dev. **14**, 214 (1970).
[36]M. W. Shafer, J. Appl. Phys. **36**, 1145 (1965).
[37]N. M. Souza-Neto, D. Haskel, Y.-C. Tseng, and G. Lapertot, Phys. Rev. Lett. **102**, 057206 (2009).
[38]P. W. Anderson, Phys. Rev. **115**, 2 (1959).
[39]V. Goian, S. Kamba, J. Hlinka, P. Vanek, A. A. Belik, T. Kolodiazhnyi, and J. Petzelt, Eur. Phys. J. B **71**, 429 (2009).
[40]V. V. Shvartsman, P. Borisov, W. Kleemann, S. Kamba, and T. Katsufuji, Phys. Rev. B **81**, 064426 (2010).
[41]K. Momma and F. Izumi, J. Appl. Crystallogr. **41**, 653 (2008).